Avrupa Bilim ve Teknoloji Dergisi
Sayı 25, S. 1-5, Ağustos 2021

Araştırma Makalesi

www.ejosat.com ISSN:2148-2683

European Journal of Science and Technology
No. 25, pp. 1-5, August 2021

Research Article

A Finite Element Method Study of Polymer Exchange Membrane Fuel Cell End Plate Materials by Using Arcan Specimen

Adem Avcu[1*], Gökhan Tüccar[2], Naghdali Choupani[3]

[1*] Adana Alparslan Türkeş Science and Technology University, Faculty of Engineering, Mechanical Engineering Department, Adana, Turkey (ORCID: 0000-0001-9981-5311), ademavcu01@gmail.com
[2] Adana Alparslan Türkeş Science and Technology University, Faculty of Engineering, Mechanical Engineering Department, Adana, Turkey (ORCID: 0000-0003-3041-299X), gtuccar@atu.edu.tr
[3] Adana Alparslan Türkeş Science and Technology University, Faculty of Engineering, Mechanical Engineering Department, Adana, Turkey (ORCID: 0000-0001-7872-6408), nchoupani@atu.edu.tr

(First received 11 December 2020 and in final form 1 May 2021)

(**DOI:** 10.31590/ejosat.837843)

ATIF/REFERENCE: Avcu, A., Tüccar, G. & Choupani, N. (2021). A Finite Element Method Study of Polymer Exchange Membrane Fuel Cell End Plate Materials by Using Arcan Specimen. *European Journal of Science and Technology*, (25), 1-5.

Abstract

In the current days, fuel cells are more preferred to generate electricity due to their positive sides. Because, if they use hydrogen and oxygen as fuel, they only produce electricity, heat, and water. This property of fuel cells is significant because it prevents environmental and chemical pollution, therefore, they contribute positively to the environment. In addition, they have more positive aspects such as having no moving or rotating parts. Therefore, they don't require mechanical maintenance and don't make noise. Besides, they can be used in a wide range of areas as mobile and stationary power sources for electricity generation. There are many fuel cell types but proton exchange membrane fuel cell (PEMFC) is more common than the other fuel cell types. It consists of parts such as an endplate, bipolar flow plate, gas diffusion layer, catalyst layer, and membrane. End plates are located on the outer side of PEMFC and hold together its stacks. In the design of the endplates, the state of fracture energy should be considered in different loading conditions. Because the material may fail if it is designed only for the strength of materials concepts. In this paper, pure mode I, pure mode II and mixed mode fracture energy behavior of different materials were investigated numerically by using Arcan specimen.

Keywords: PEMFC, End plate, Fracture energy, Strain energy release rate, Arcan specimen.

Polimer Değişim Membranlı Yakıt Hücresi Uç Plakası Malzemelerinin Arcan Numunesi Kullanılarak Sonlu Eleman Yöntemi ile Çalışılması

Öz

Günümüzde yakıt pilleri, olumlu yönleri nedeniyle elektrik üretmek için daha çok tercih edilmektedir. Çünkü yakıt pilleri, yakıt olarak hidrojen ve oksijeni kullanırsa sadece elektrik, ısı ve su üretir. Yakıt pillerinin bu özelliği, çevre ve kimyasal kirlenmeyi engellemesi nedeniyle önemlidir, bu nedenle çevreye olumlu katkı sağlarlar. Ayrıca hareketli veya dönen parçaların olmaması gibi olumlu yönleri de vardır. Bu nedenle mekanik bakım gerektirmez ve gürültü oluşturmazlar. Ayrıca elektrik üretimi için mobil ve sabit güç kaynağı olarak çok çeşitli alanlarda kullanılabilirler. Birçok yakıt hücresi türü vardır, ancak proton değişim membranlı yakıt hücresi (PEMFC) diğer yakıt hücresi türlerinden daha yaygındır. Bir uç plakası, iki kutuplu akış plakası, gaz difüzyon katmanı, katalizör katmanı ve membran gibi parçalardan oluşur. Uç plakaları, PEMFC'nin dış tarafında bulunur ve hücre yığınlarını bir arada tutar. Uç plakaların tasarımında, farklı yükleme koşullarında kırılma enerjisi durumu dikkate alınmalıdır. Çünkü malzeme, yalnızca malzeme mukavemeti yaklaşımı ile tasarlanırsa başarısız olabilir. Bu makalede, Arcan numunesi kullanılarak farklı malzemelerin yalın mod I, yalın mod II ve karışık mod kırılma enerjileri ve malzemelerin kırılma davranışları sayısal olarak incelenmiştir.
Anahtar Kelimeler: PEMFC, Uç plaka, Kırılma enerjisi, Gerinim enerjisi boşalma oranı, Arcan numunesi.

[*] Corresponding Author: ademavcu01@gmail.com

1. Introduction

Energy production and supply have become one of the most important issues of humanity with the start of the industrial revolution. Fossil fuel has been used in all areas of industry and it is still used, but it causes environmental pollution and it has a bad influence on climate change. The increment of global warming has led to seek clean and renewable energy in the time. In renewable and clean energy sources, fuel cells have attracted much attention in current years owing to noiseless, low maintenance requirement, high energy efficiency and low emissions. Additionally, they can be used in wide range areas including stationary and mobile power source such as automotive, marine and aviation sectors [1-4].

Proton exchange membrane fuel cell (PEMFC) is more widespread than other fuel cell types due to following advantages: low temperature operation, high efficiency, nearly zero pollutants, simple structure and fast start up [1, 5-8]. It basically consists of end plate, bipolar flow plate, gas diffusion layer, catalyst layer and membrane. The PEMFC and its parts are given in Figure 1 [9]. Generally, gas diffusion layer, catalyst layer and membrane are combined with together hot pressing process and it is named as membrane electrode assembly (MEA) [10-15]. The main work principle of PEMFC is hydrogen protons transfer by MEA that affects performance of PEMFC. Also, MEA is affected from clamping pressure. The clamping pressure is provided by end plates that are located on the outer side of the fuel cell stacks. They should have properties such as low density, high mechanical strength, electrochemical stability, electrical insulation. Therefore, an appropriate material selection is important to prevent performance drop of PEMFC [13-15].

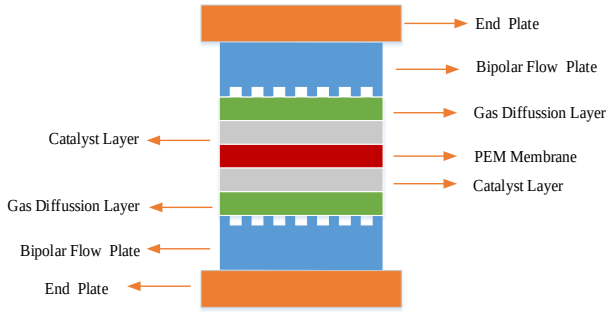

Figure 1. The PEMFC and its parts

Fracture energy is used to determine what kind of failure may occur under different loading conditions. There are three fracture energy modes that are mode I (opening), mode II (shearing) and mode III (tearing) [16-18]. Fracture modes are given in Figure 2 [9]. Fuel cells are used in different areas so they can be exposed to one fracture mode or combining of them. Generally, evaluation of fracture energy is obtained using only one method. But, Arcan specimen provides facility to observe fracture energy of the materials at mode I, mode II and mixed mode load conditions [19, 20].

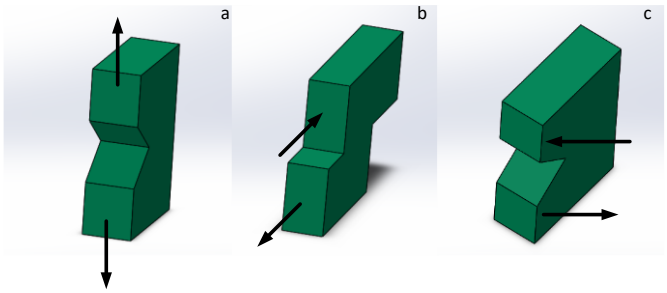

Figure 2. Fracture modes: (a) mode I (opening), (b) mode II (shearing), (c) mode III (tearing)

In this paper, numerical fracture analyses were carried out to find failure of end plate materials by using Abaqus package program. The materials were examined to obtain mode I, mode II and mixed mode fracture energy values under different loading angles by using Arcan specimen. As a result of the analyses, an appropriate material was determined for end plate.

2. Material and Method

End plates provides sufficient pressure to hold stacks together. They can be made from metal and non-metal materials. To provide proper pressure, they should have features such as high mechanical strength, electrical insulation, corrosion resistance and low density [13-16]. In this study, different materials are investigated for the most appropriate end plate material. They are selected as boron carbide (B_4C), E-glass/ epoxy, brass, Kevlar-49/ epoxy, NiAl alloy, SiC alloy, TiAl6V4 and T700/ epoxy. Mechanical properties of the materials used for numerical analysis are listed in Table 1. The notation used is as follows: elastic modulus in x-direction (E_1), elastic modulus in y-direction (E_2), elastic modulus in z-direction (E_3), shear modulus in x-y direction (G_{12}), shear modulus in x-z direction (G_{13}), shear modulus in y-z direction (G_{23}), poisson's ratio in x-y direction (υ_{12}), poisson's ratio in x-z direction (υ_{13}), poisson's ratio in y-z direction (υ_{23}). Stress intensity factors and strain energy release rates of the materials were obtained numerically by using the Abaqus package program. Arcan specimen gives facility to obtain mode I, mode II and mixed mode fracture energy under different loading angles. Also, 1000 N load was applied to different materials by using Arcan specimen. The specimen models prepared with different fracture modes are shown in Figure 3.

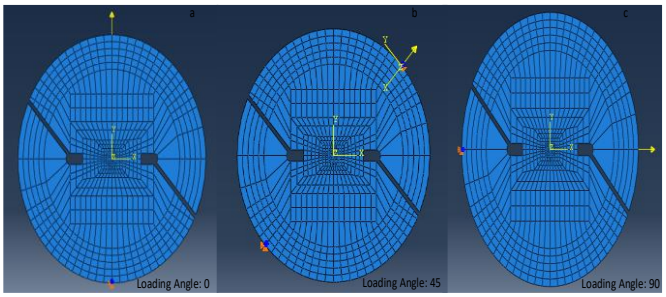

Figure 3. The Arcan specimen models prepared for different fracture modes: (a) pure mode I, (b) mixed mode, (c) pure mode II

Metals and their alloys materials are assumed as isotropic materials. The fracture energy of an isotropic material can be calculated by using Equations (1) and (2) for plane strain conditions [17]. The notation used is as follows: mode I stress

intensity factor (K_I), mode II stress intensity factor (K_{II}), strain energy release rate mode I (G_I), strain energy release rate mode II (G_{II}), elastic modulus (E) and poisson's ratio (ν) [27].

$$G_I = K_I^{\,2}/\overline{E}$$
$$G_{II} = K_{II}^{\,2}/\overline{E} \quad (1)$$

$$\overline{E} = E/(1-\nu^2) \quad (2)$$

Composite specimens are considered as orthotropic linear elastic materials. Strain energy release rates (G_I, G_{II}) and the effective moduli (E_I, E_{II}) are given in Equations (3) and (4), respectively [18, 19]. Linear elastic fracture mechanics (LEFM) is a useful approach to investigate cracks on composites. Deformation of orthotropic linear elastic material is stated using generalized Hooke's law that is given in Equation (5). Elastic constants are stated as in Equation (6) [9, 18].

$$G_I = K_I^{\,2}/E_I$$
$$G_{II} = K_{II}^{\,2}/E_{II} \quad (3)$$

$$E_I = \sqrt{\frac{2}{b_{11}b_{22}}}\cdot\frac{1}{\sqrt{\sqrt{\frac{b_{22}}{b_{11}}}+\frac{2b_{12}+b_{66}}{2b_{11}}}}$$
$$E_{II} = \frac{\sqrt{2}}{b_{11}}\cdot\frac{1}{\sqrt{\sqrt{\frac{b_{22}}{b_{11}}}+\frac{2b_{12}+b_{66}}{2b_{11}}}} \quad (4)$$

$$\begin{pmatrix}\varepsilon_x\\ \varepsilon_y\\ \varepsilon_z\\ \gamma_{yz}\\ \gamma_{xz}\\ \gamma_{xy}\end{pmatrix} = \begin{pmatrix}a_{11} & a_{12} & a_{13} & a_{14} & a_{15} & a_{16}\\ a_{21} & a_{22} & a_{23} & a_{24} & a_{25} & a_{26}\\ a_{31} & a_{32} & a_{33} & a_{34} & a_{35} & a_{36}\\ a_{41} & a_{42} & a_{43} & a_{44} & a_{45} & a_{46}\\ a_{51} & a_{52} & a_{53} & a_{54} & a_{55} & a_{56}\\ a_{61} & a_{62} & a_{63} & a_{64} & a_{65} & a_{66}\end{pmatrix}\begin{pmatrix}\sigma_x\\ \sigma_y\\ \sigma_z\\ \tau_{yz}\\ \tau_{xz}\\ \tau_{xy}\end{pmatrix} \quad (5)$$

$$a_{11} = \frac{1}{E_x};\ a_{22} = \frac{1}{E_y};\ a_{33} = \frac{1}{E_z};\ a_{44} = \frac{1}{G_{yz}};\ a_{55} = \frac{1}{G_{xz}};$$
$$a_{66} = \frac{1}{G_{xy}};\ a_{12} = a_{21} = -\frac{v_{xy}}{E_x} = -\frac{v_{yx}}{E_y};$$
$$a_{13} = a_{31} = -\frac{v_{xz}}{E_x} = -\frac{v_{zx}}{E_z};\ a_{23} = a_{32} = -\frac{v_{yz}}{E_y} = -\frac{v_{zy}}{E_z} \quad (6)$$

For plane strain condition $\varepsilon_z = \gamma_{yz} = \gamma_{xz} = 0$, the generalized Hooke's law turns into Equation (7)

$$\begin{pmatrix}\varepsilon_x\\ \varepsilon_y\\ \gamma_{xy}\end{pmatrix} = \begin{pmatrix}b_{11} & b_{12} & b_{16}\\ b_{12} & b_{22} & b_{26}\\ b_{16} & b_{26} & b_{66}\end{pmatrix}\begin{pmatrix}\sigma_x\\ \sigma_y\\ \tau_{xy}\end{pmatrix} \quad (7)$$

Where the constants b_{ij} are defined in terms of a_{ij} of the compliance matrix, which are given in Equations (8) and (9).

$$b_{ij} = a_{ij} - \frac{a_{i3}a_{j3}}{a_{33}} \text{ (i, j=1, 2, 4, 5, 6)} \quad (8)$$

$$a_{16} = a_{26} = a_{36} = a_{45} = 0,\ b_{16} = b_{26} = 0,$$
$$b_{11} = \frac{a_{11}a_{33}-a_{13}^2}{a_{33}},\ b_{12} = \frac{a_{12}a_{33}-a_{13}a_{23}}{a_{33}},\ b_{22} = \frac{a_{22}a_{33}-a_{23}^2}{a_{33}},$$
$$b_{66} = \frac{a_{66}a_{33}-a_{36}^2}{a_{33}} \quad (9)$$

Total strain energy release rate of material (G_T) is given in Equation (10).

$$G_T = G_I + G_{II} \quad (10)$$

Table 1. Elastic properties of the metallic alloys, ceramics and composite materials used.

Material	E_1 [GPa]	E_2 [GPa]	E_3 [GPa]	G_{12} [GPa]	G_{13} [GPa]	G_{23} [GPa]	υ_{12}	υ_{13}	υ_{23}
B_4C [21]	434	434	434	114.21	114.21	114.21	0.19	0.19	0.19
Brass [25]	101	101	101	38.55	38.55	38.55	0.31	0.31	0.31
E-glass/ epoxy [22]	41	12	12	5.50	5.50	3.50	0.28	0.28	0.50
Kevlar-49/ epoxy [22]	80	5.50	5.50	2.20	2.20	1.80	0.34	0.34	0.4
NiAl [23]	186	186	186	71	71	71	0.31	0.31	0.31
SiC [23]	450	450	450	184.43	184.43	184.43	0.22	0.22	0.22
TiAl6V4 [26]	113.80	113.80	113.80	42.46	42.46	42.46	0.34	0.34	0.34
T700/ epoxy [24]	132	10.30	10.30	6.50	6.50	3.91	0.25	0.25	0.38

3. Results and Discussion

Kevlar-49/ epoxy exhibited the highest strain energy release at mode I (*GI*) among all materials. But, when it comes to strain energy release at mode II (*GII*), E-glass/ epoxy was the material having the highest value. The strain energy release rates of the materials can be seen in Table 2 for pure mode I, mode II and total of mode I and II (G_I, G_{II} and $G_T = G_I + G_{II}$), respectively. The selected materials underwent different deformation modes due to different loading conditions. Additionally, they gave different results in terms of stress intensity factor and strain energy release rate characteristically because of dissimilar mechanical properties. Arcan specimen deformation results are given in Figure 4.

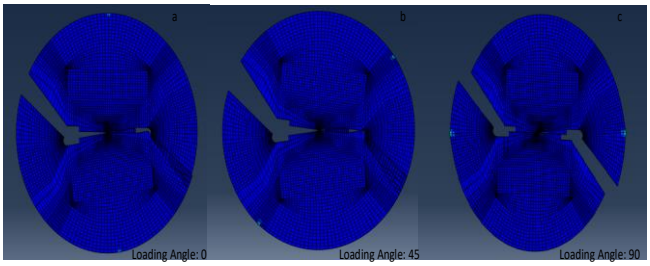

Figure 4. The Arcan specimen model deformations after different loading conditions: (a) pure mode I, (b) mixed mode, (c) pure mode II

Table 2. Strain energy release rates of the materials

Material	G_I	G_{II}	G_T
Kevlar-49/ epoxy	133.22	4.86	138.08
T700/ epoxy	95.11	3.60	98.71
E-glass/ epoxy	81.39	4.97	86.36
Brass	13.36	1.88	15.24
TiAl6V4	11.71	1.68	13.39
NiAl	7.61	1.17	8.78
B_4C	3.68	0.61	4.29
SiC	3.51	0.59	4.10

When all materials are investigated at mode I (G_I) loading condition, all of materials have the highest value at pure mode I fracture energy. As getting closer to mode II condition, mode I (G_I) starts to decrease progressively. When loading angle reaches to pure mode II condition, mode I (G_I) drops off to its the lowest value. Figure 5 shows that Kevlar-49/ epoxy gave the highest G_I value at mode I condition. On the other hand, SiC showed the lowest G_I value among the materials.

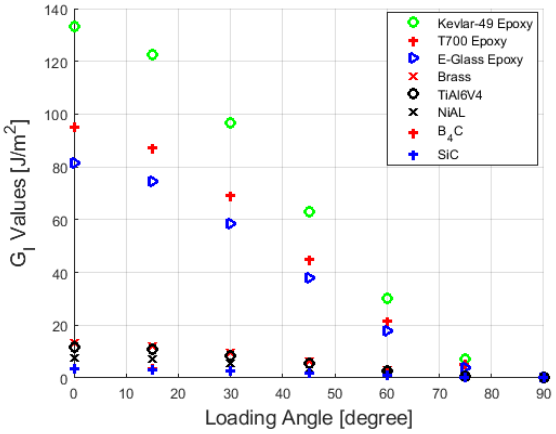

Figure 5. G_I versus loading angle graph

It can be seen that by approaching to pure mode II condition, G_{II} increases gradually. When loading angle reaches to pure mode II condition, G_{II} reaches to its the highest value. E-glass/ epoxy exhibited the highest strain energy release rate among the materials at mode II condition. SiC gave the lowest G_{II} value. Mode II (G_{II}) versus loading angle graph is given in Figure 6.

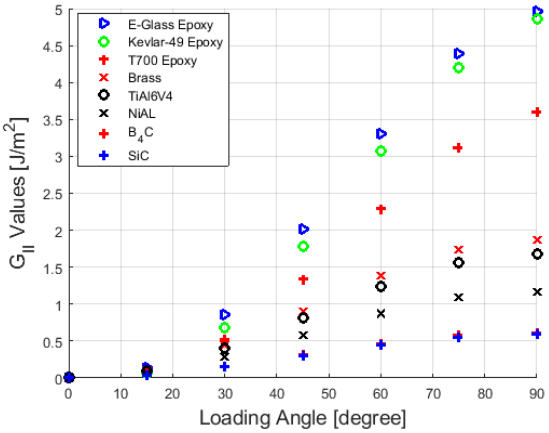

Figure 6. G_{II} versus loading angle graph

Total strain energy release rate of the material is summation of mode I and mode II strain energy release rates and it is expressed as G_T. All the materials had the maximum G_T at pure mode I condition. When approaching to pure mode II condition, G_T started to decrease gradually. But, G_T reached its lowest value at pure mode II point. It can be seen that Kevlar-49/ epoxy had the highest G_T at mode I condition. SiC had the lowest G_T value among the materials. Total strain energy release rate relative to angle is shown in Figure 7.

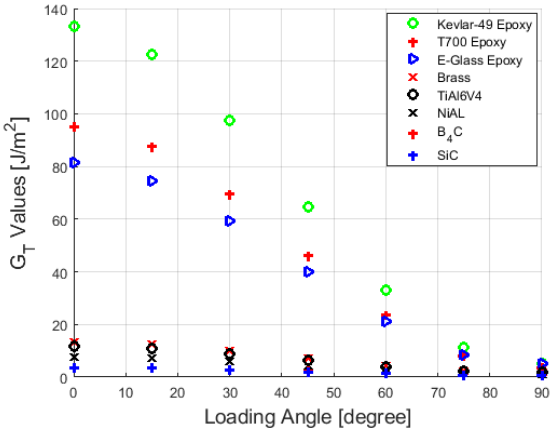

Figure 7. G_T versus loading angle graph

4. Conclusion

In this study, eight different materials were investigated to decide which one is more suitable for PEMFC end plate. Arcan specimen finite element model was used to calculate the fracture energy. 1000 N load was applied to find fracture energy of the materials for mode I, mode II and mixed modes. Loading angle was increased in increments of 15º, starting from 0º (pure mode I) until reaching 90º (pure mode II). According to the results, mode I strain release rate (G_I) was higher than mode II strain release rate (G_{II}) for all materials. In addition, Kevlar-49/epoxy had the highest G_I value among the other materials. E-glass/ epoxy had the highest G_{II} value. It can be seen that for isotropic materials, the increase in stiffness leads to a reduction of total strain energy release rate (i.e., an increase in the fracture resistance). The total strain energy release rate for Kevlar-

49/epoxy was higher than that of other composite materials, which leads to a reduction of fracture resistance in this material. A higher fracture resistance was obtainable with E-glass/epoxy composite which resulted in a reduction the total strain energy release rate. In this paper, finite element fracture analyses were performed to explain some of the issues related to the fracture energy of fuel cell end plate materials using Arcan samples. There is still a considerable activity in this area because of the importance of the issue. In order to expand the understanding of fractures and to more accurately determine the fracture criteria for PEMFC materials, additional experimental analyses should be performed using the mixed mode Arcan fracture test.

References

Baroutaji, A., Carton, J. G., Sajjia, M., & Olabi, A. G. (2015). Materials in PEM fuel cells.

Van Biert, L., Godjevac, M., Visser, K., & Aravind, P. V. (2016). A review of fuel cell systems for maritime applications. *Journal of Power Sources*, *327*, 345-364.

Gencoglu, M. T., & Ural, Z. (2009). Design of a PEM fuel cell system for residential application. *International Journal of Hydrogen Energy*, *34*(12), 5242-5248.

Wang, Y., Chen, K. S., Mishler, J., Cho, S. C., & Adroher, X. C. (2011). A review of polymer electrolyte membrane fuel cells: Technology, applications, and needs on fundamental research. *Applied energy*, *88*(4), 981-1007.

Vishnyakov, V. M. (2006). Proton exchange membrane fuel cells. *Vacuum*, *80*(10), 1053-1065.

Qin, C., Wang, J., Yang, D., Li, B., & Zhang, C. (2016). Proton exchange membrane fuel cell reversal: a review. *Catalysts*, *6*(12), 197.

Elden, G., & Mert, T. A. Ş. (2014). Numerical Investigation of Anisotropic Electrical Conductivity Effects in Proton Exchange Membrane Fuel Cell. *Avrupa Bilim ve Teknoloji Dergisi*, (Special Issue), 2-6.

Haile, S. M. (2003). Fuel cell materials and components. *Acta Materialia*, *51*(19), 5981-6000.

Avcu, A . (2020). Fracture energy comparison of aluminum and boron composites for fuel cell end plates. *International Journal of Energy Applications and Technologies*, 7 (4), 149-153.

Wilberforce, T., El Hassan, Z., Ogungbemi, E., Ijaodola, O., Khatib, F. N., Durrant, A., ... & Olabi, A. G. (2019). A comprehensive study of the effect of bipolar plate (BP) geometry design on the performance of proton exchange membrane (PEM) fuel cells. *Renewable and Sustainable Energy Reviews*, *111*, 236-260.

Moreira, J., Sebastian, P. J., Ocampo, A. L., Castellanos, R. H., Cano, U., & Salazar, M. D. (2002). Dependence of PEM fuel cell performance on the configuration of the gas diffusion electrodes. *Journal of New Materials for Electrochemical Systems*, *5*(3), 173-176.

Touhami, S., Mainka, J., Dillet, J., Taleb, S. A. H., & Lottin, O. (2019). Transmission line impedance models considering oxygen transport limitations in polymer electrolyte membrane fuel cells. *Journal of the Electrochemical Society*, *166*(15), F1209.

Kim, J. S., Park, J. B., Kim, Y. M., Ahn, S. H., Sun, H. Y., Kim, K. H., & Song, T. W. (2008). Fuel cell end plates: a review. *International Journal of Precision Engineering and Manufacturing*, 9(1), 39-46.

Asghari, S., Shahsamandi, M. H., & Khorasani, M. A. (2010). Design and manufacturing of end plates of a 5 kW PEM fuel cell. *International Journal of Hydrogen Energy*, 35(17), 9291-9297.

Yu, H. N., Kim, S. S., & Do Suh, J. (2010). Composite endplates with pre-curvature for PEMFC (polymer electrolyte membrane fuel cell). *Composite Structures*, *92*(6), 1498-1503.

Shameli, M., & Choupani, N. (2016). Fracture criterion of woven glass-epoxy composite using a new modified mixed-mode loading fixture. *International Journal of Applied Mechanics*, *8*(02), 1650015.

Choupani, N. (2009). Characterization of fracture in adhesively bonded double-lap joints. *International Journal of Adhesion and Adhesives*, *29*(8), 761-773.

Choupani, N, (2008), Experimental and numerical investigation of the mixed-mode delamination in Arcan laminated specimens, *Materials Science and Engineering: A*, 478, 229-242.

Hossein Abadi, R., Refah Torun, A., Mohammadali Zadeh Fard, A., & Choupani, N. (2020). Fracture characteristics of mixed-mode toughness of dissimilar adherends (cohesive and interfacial fracture). *Journal of Adhesion Science and Technology*, *34*(6), 599-615.

Rahmani, A., & Choupani, N. (2019). Experimental and numerical analysis of fracture parameters of adhesively bonded joints at low temperatures. *Engineering Fracture Mechanics*, *207*, 222-236.

Kuliiev, R., Orlovskaya, N., Hyer, H., Sohn, Y., Lugovy, M., Ha, D., ... & Blugan, G. (2020). Spark Plasma Sintered B4C—Structural, Thermal, Electrical and Mechanical Properties. *Materials*, *13*(7), 1612.

Kasavajhala, A. R. M., & Gu, L. (2011). Fracture analysis of Kevlar-49/epoxy and e-glass/epoxy doublers for reinforcement of cracked aluminum plates. *Composite structures*, *93*(8), 2090-2095.

Hsieh, C. L., & Tuan, W. H. (2005). Elastic properties of ceramic–metal particulate composites. *Materials Science and Engineering: A*, *393*(1-2), 133-139.

Hassan, S. A., Santulli, C., Yahya, M. Y. B., Gang, C. L., & Abu, B. M. N. (2018). The potential of biomimetics design in the development of impact resistant material. *FME Transactions*, *46*(1), 108-116.

Acosta-Flores, M., Jiménez-López, E., Chávez-Castillo, M., Molina-Ocampo, A., Delfín-Vázquez, J. J., & Rodríguez-Ramírez, J. A. (2019). Experimental method for obtaining the elastic properties of components of a laminated composite. *Results in Physics*, *12*, 1500-1505.

Schubert, A., Zeidler, H., Jahn, S. F., Flemmig, S., & Schulze, R. (2014). Vibration Analysis of an Ultrasonic-Assisted Joining System. *Procedia Engineering*, *69*, 1021-1028.

Avcu, A , Choupani, N , Tüccar, G . (2020). A Numerical Investigation of The Fracture Energy of Materials for Fuel Cell End Plates. *European Mechanical Science*, 5 (2), 56-63.